

A multiple-scale simulation of variations in atmospheric carbon dioxide using a coupled biosphere-atmospheric model

Melville E. Nicholls,¹ A. Scott Denning,¹ Lara Prihodko,¹ Pier-Luigi Vidale,² Ian Baker,¹ Kenneth Davis,³ and Peter Bakwin⁴

Received 22 December 2003; revised 26 May 2004; accepted 9 July 2004; published 29 September 2004.

[1] Variations of atmospheric CO₂ at regional scales are becoming increasingly important in understanding regional carbon budgets, yet the processes that drive them remain relatively unexplored. A simulation was conducted to test a coupled biosphere-atmospheric model (SiB2-RAMS), by comparing with measurements made at the WLEF-TV tower in Wisconsin, and to investigate some of the mechanisms leading to CO₂ variability, both on local and regional scales. The simulation was run for a 5-day period from 26 to 30 July 1997. Multiple nested grids were employed, which enabled mesoscale features to be simulated and which resolved small-scale features in the vicinity of the WLEF tower. In many respects the model was successful at simulating observed meteorological variables and CO₂ fluxes and concentrations. The two most significant deficiencies were that excessive nighttime cooling occurred on two of the nights and that late afternoon uptake of CO₂ was larger than observed. Results of the simulation suggest that in addition to biological processes causing variations in CO₂ concentrations at the WLEF site other factors, such as small nearby lakes, turbulence induced by vertical wind shear, boundary layer thermals, and clouds, also had significant impacts. These factors add to the difficulty of interpreting CO₂ measurements. Regional-scale patterns of CO₂ variability caused by meteorological processes were also identified. Katabatic winds had a significant effect by causing respired CO₂ to pool in valleys and along the shores of the Great Lakes during the night. Furthermore, a large diurnal cycle of CO₂ concentration occurred over the lakes, which appeared to be mainly due to the combined action of katabatic winds, ambient winds, and the lake breeze circulation. These results suggest that meteorological processes associated with the complex terrain in this region leads to substantial CO₂ advection. Therefore meteorological as well as biological processes are likely to be important causes of regional-scale CO₂ variability in the Great Lakes region. A sensitivity test conducted to examine the differences between using a turbulent kinetic energy based subgrid-scale scheme versus a deformation-type subgrid-scale scheme showed advantages and disadvantages to both approaches. Our results suggest that continuous records of CO₂ variability measured over heterogeneous continental regions must be interpreted with caution because of the impact of mesoscale circulations on the concentration time series.

INDEX TERMS: 3322 Meteorology and Atmospheric Dynamics: Land/atmosphere interactions; 3337 Meteorology and Atmospheric Dynamics: Numerical modeling and data assimilation; 4805 Oceanography: Biological and Chemical: Biogeochemical cycles (1615); **KEYWORDS:** carbon budgets, carbon dioxide, biosphere, regional-scale modeling, missing sink, carbon dioxide fluxes

Citation: Nicholls, M. E., A. S. Denning, L. Prihodko, P.-L. Vidale, I. Baker, K. Davis, and P. Bakwin (2004), A multiple-scale simulation of variations in atmospheric carbon dioxide using a coupled biosphere-atmospheric model, *J. Geophys. Res.*, 109, D18117, doi:10.1029/2003JD004482.

¹Department of Atmospheric Science, Colorado State University, Fort Collins, Colorado, USA.

²Institute for Atmospheric and Climate Science, ETH Zurich, Zurich, Switzerland.

³Department of Meteorology, Pennsylvania State University, University Park, Pennsylvania, USA.

⁴Climate Monitoring and Diagnostics Laboratory, NOAA, Boulder, Colorado, USA.

1. Introduction

[2] Understanding and quantifying the global carbon budget is of considerable importance if the magnitude of possible future global warming is to be accurately predicted. Observations of the north-south gradient of atmospheric CO₂ suggest that there is a large terrestrial carbon sink in the Northern Hemisphere [*Tans et al.*, 1990; *Intergovernmental Panel on Climate Control (IPCC)*, 2001]. A recent intercomparison study of tracer transport

inversions reported by *Gurney et al.* [2003] indicates a northern land sink distributed relatively evenly among the Northern Hemisphere continents. These global inversions employed large-scale general circulation models (GCMs). As more extensive CO₂ data sets become available, the possibility exists that regional-scale atmospheric models could be used to bring a sharper focus as to where the sources and sinks of CO₂ over a particular continent actually occur. Regional atmospheric data collected at high spatial and temporal resolution are envisioned under the North American Carbon Program (NACP) [*Wofsy and Harris, 2002*] as a means to test mechanistic hypotheses about sources and sinks. Multiple-scale atmospheric models which use nested grids to span a wide range of spatial scales, and which are coupled to biosphere models to provide surface fluxes of CO₂, may lead to a better understanding of the processes causing variations in atmospheric CO₂ at both the local and regional scales. This would help in the interpretation of measurements made at tower sites and by aircraft, as well as providing valuable information of how accurately regional-scale models can be expected to transport CO₂.

[3] In this study, a biosphere model was coupled with a multiple-scale atmospheric model and tested to assess its ability to simulate observed CO₂ concentration, CO₂ flux and other meteorological quantities at a tall tower site. The site was chosen because measurements made from the mid-boundary layer reflect the influence of a large heterogeneous area. The coupled model incorporates parameterizations of many physical and biological processes and close comparison with observations is important for evaluating the validity of these parameterizations. This multiple-scale simulation which encompasses a 600 km by 600 km area and which is run for a five day period, can be viewed as a step toward the utilization of regional-scale coupled biosphere-atmospheric models which may encompass most or all of the North American continent and be run for periods of a few months to a few years.

[4] This study has five main objectives. The first is to evaluate the coupled biosphere model by comparing the results of the simulation with local observations made at the WLEF-TV tower near Park Falls, Wisconsin. The second is to use the model to examine larger regional patterns of CO₂ variability, for which there are limited observations. The third is to gain a better understanding of some of the processes that lead to both local and regional-scale CO₂ variability. The fourth is to explore the signal-to-noise ratio of CO₂ variability. In this respect, an important purpose of making CO₂ measurements is to relate variability of atmospheric CO₂ concentrations to variability in the surface fluxes of CO₂, or the “signal”. There is however “noise” in the measurements since the variation of CO₂ concentration depends on meteorological, as well as biological processes. From the point of view of estimation of fluxes, most of this noise actually arises from the inability of models to capture details of atmospheric transport [*Engelen et al., 2002; Gurney et al., 2003; Gerbig et al., 2003*]. In this study, we investigate the relative importance of surface biogeochemistry and meteorology in causing variations in measured CO₂ concentrations. The final objective is to conduct model sensitivity tests to some of the physical parameterizations; experiments were conducted to examine

the effect of including cloud microphysics and of using different types of subgrid-scale turbulent schemes.

[5] In a previous study, *Denning et al.* [2003] reported on results of the coupled Simple Biosphere-Regional Atmospheric Modeling System (SiB2-RAMS). Results of a high resolution (horizontal grid increment of 100 m) two-dimensional simulation were compared with observations at the WLEF-TV tower, for 26 and 27 July 1997. Generally, the model compared favorably with observations and showed in detail the features of the CO₂ concentration field in the evolving planetary boundary layer. One discrepancy was that the model predicted the development of a CO₂ minimum in a shallow layer next to the surface, just before sunset. This arose because of a tendency of the model to overestimate late afternoon canopy activity (transpiration and photosynthesis), leading to persistent CO₂ uptake under a stable layer that forms about an hour too early. This phenomenon may be attributable to misrepresentation of the extinction of direct beam radiation in SiB2 and was also noted by *Baker et al.* [2003].

[6] The previous two-dimensional study was limited in its ability to simulate observed variables at the WLEF site since it did not include large-scale advection or land surface variability. In this paper, these limitations have been removed, first by running a three-dimensional multiple nested grid simulation which is capable of simulating large mesoscale features and which telescopes down to resolve very small scale features in the vicinity of the WLEF tower. Additionally, by utilizing high-resolution vegetation, surface elevation and meteorological data sets for model initialization and boundary conditions. The more realistic model configuration used in this study allows for a more rigorous evaluation of its performance when compared with observations at the WLEF site. The size of the domain has been made large enough for regional-scale patterns of CO₂ variability to be examined. To help identify the processes leading to atmospheric CO₂ variability model output data was written out at a frequent time interval so that the evolution of the meteorological fields, surface fluxes and CO₂ concentration could be examined. Additionally, model sensitivity tests have been conducted in some instances to elucidate the factors involved.

[7] In section 2, the coupled biosphere-atmospheric model is described with emphasis on additional model features not used in the previous study. In section 3, the case chosen for simulation is discussed. In section 4, details are given of the model configuration, and the data sets and procedures used for model initialization and boundary conditions. In section 5, the model experiments are described. In section 6 results are discussed, first for the control run, then for the simulation with clouds, and finally for the simulation that employs an alternative subgrid-scale turbulence approach. Conclusions are presented in section 7.

2. Model Descriptions

[8] The atmospheric model used in this study is the Colorado State Regional Atmospheric Modeling System (RAMS) and is discussed by *Pielke et al.* [1992], *Nicholls et al.* [1995], and *Cotton et al.* [2003]. The biosphere model is the Simple Biosphere (SiB) Model developed by *Sellers et al.* [1986], which has undergone substantial modification

[*Sellers et al.*, 1996a, 1996b], and is now referred to as SiB2. Details of the coupled model can be found in the previous study by *Denning et al.* [2003]. This discussion focuses on the turbulence closure options and additional model features pertinent to this particular study.

[9] One of the turbulence closure options available in RAMS which is used in this study, is the first-order scheme of *Smagorinsky* [1963], which uses a deformation-based mixing coefficient. The scheme includes optional dependencies on the Brunt-Vaisala frequency [*Hill*, 1974] and the Richardson number [*Lilly*, 1962], which together enhance diffusion in unstable conditions and reduce diffusion in stable conditions. The Lilly and Hill modifications were originally designed for use without one another, although in practice it has been found that the added vertical diffusion in unstable air obtained by using them together is usually desirable. This option gives reasonable results for both mesoscale and small-scale large eddy simulations. Another option available to RAMS uses the *Mellor and Yamada* [1982] scheme for the vertical diffusion, which employs a prognostic turbulent kinetic energy (TKE), and uses the Smagorinsky scheme for horizontal diffusion. This option is applicable for mesoscale simulations when turbulent boundary layer eddies are not resolved. Additionally, there is an option for parameterizing horizontal and vertical diffusion according to *Deardorff's* [1980] scheme, which also employs a prognostic TKE. This scheme is intended only for the specific purpose of performing large eddy simulations in which it is assumed that resolved eddy motions in the model perform most of the eddy transport. This option was used in the previous high-resolution study reported by *Denning et al.* [2003]. These two latter schemes which employ a prognostic TKE are used in conjunction with one another in this study, an approach that has also been used by *Costigan* [1992]. The idea of this approach is to apply the Mellor-Yamada scheme on the coarse grid(s) which resolve the large quasi-horizontal mesoscale eddies and the Deardorff scheme on the fine grid(s) which resolve some of the much smaller three-dimensional turbulent eddies in the boundary layer. Unfortunately, neither scheme was designed for use at a scale between about 500 m to 5 km, and this scale is of course, spanned by the nested grids in this study. At this intermediate scale a turbulence parameterization designed to model all of the vertical transport in the boundary layer is not really appropriate, since the turbulence energy is partly resolved. This may create an artificial interaction between the resolved and parameterized turbulence. Conversely, a subgrid-scale scheme that makes the assumption that resolved eddy motions perform most of the eddy transport will likely underestimate vertical mixing at that scale. Therefore, as will be discussed in section 5, experiments were conducted to see which one of the schemes works best at this intermediate scale.

[10] The two-way interactive multiple nested grid scheme developed by *Clark and Farley* [1984] is used in this study. This enables the representation of large-scale features and by using successively finer grids, telescoping down to smaller scales in the region of interest. A terrain-following vertical coordinate is employed [*Gal-Chen and Somerville*, 1975; *Clark*, 1977]. The radiation condition discussed by *Klemp and Wilhelmson* [1978] is used at the lateral boundaries, which assumes that disturbances reaching the

boundaries move as linearly propagating gravity waves. Additionally, for this simulation which uses operational data the nudging scheme of *Davies* [1983] is used, which externally forces the lateral boundary values toward the observations during the simulation. The upper levels of the model domain are similarly nudged. RAMS has an isentropic analysis package, which performs the data analysis tasks for the initial and boundary conditions.

3. Case Description

[11] Observations were made at a Wisconsin forest site, which is the location of a 450 meter tall television transmission tower (WLEF-TV, 45°55'N, 90°10'W), in the Chequamegon National Forest, 24 km west of Park Falls, WI. The area is in a heavily forested zone of low relief. The region immediately surrounding the tower is dominated by boreal lowland and wetland forests typical of the region. The concentration of CO₂ has been measured continuously at 6 heights (11, 30, 76, 122, 244, and 396 m above the ground) since October 1994, and CO₂ flux has been measured at three heights at this tower (30, 122 and 396 m) since 1996 [*Bakwin et al.*, 1998; *Berger et al.*, 2001; *Davis et al.*, 2003].

[12] The period simulated was from 6 a.m. LST 26 July 1997 to 6 a.m. LST 31 July 1997. These dates were chosen because there were good observations for this period and because it was a relatively cloud free period, so that results would not crucially depend on the accurate modeling of complex cloud microphysical processes. The day prior to 26 July was cloudy with some precipitation. On 26 and 27 July it was very warm and humid. Winds at the WLEF site were predominantly from the west on 26 July and during the daytime on 27 July. During the night of 27 July the winds strengthened and veered bringing colder and drier air from the north. The temperature gradually warmed in the following days and the winds backed, eventually becoming southwesterly.

4. Model Configuration, Initialization, and Boundary Conditions

[13] The SiB2 model requires both time varying and time invariant vegetation parameters. Time invariant vegetation biophysical parameters, such as canopy height and leaf angle distribution, are based on values recorded in the literature and assigned to a particular biome via look-up tables [*Sellers et al.*, 1996b]. We used the 1 km vegetation classification created by *Hansen et al.* [2000] to assign these biophysical parameters across the domain. It was necessary to remap the Hansen data set to SiB2 vegetation classes in order to assign the properties. Seven land cover types are represented in the domain: deciduous broadleaf, mixed broadleaf/needleleaf forest, evergreen needleleaf, shrubs, agriculture and grasslands, bare and urban, and water. A map of these surface types at a 1 km resolution for the area is shown in Figure 1a. The biome class at the WLEF site is mixed forest. In the surrounding area there is a mixture of mainly mixed forest and deciduous broadleaf trees. Lake Superior is approximately 70 km to the north of the WLEF site and Lake Michigan farther to the southeast. To the south, shrubs, agriculture and grasslands are more common.

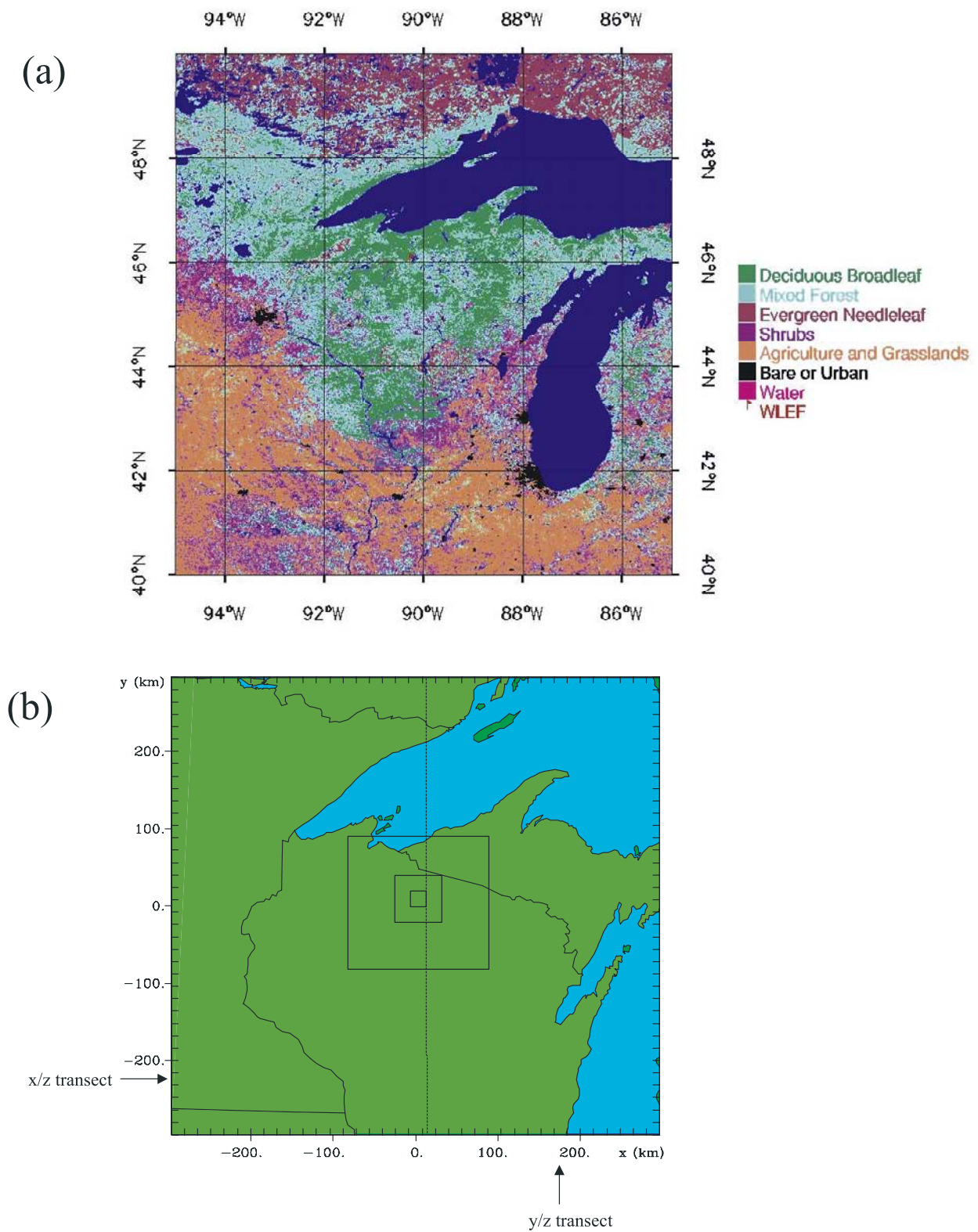


Figure 1. (a) Map of the vegetation classes for the SiB2 model. The location of the WLEF-TV tower is indicated. (b) Model domain and outline of the three nested grids. Location of transects used in Figure 13 are indicated.

Evergreen needleleaf is only significant north of Lake Superior. Time invariant soil hydraulic and thermal properties for SiB2 were calculated from the percent of sand and clay in the soil using equations from *Clapp and Hornberger* [1978] as modified by *Bonan* [1996]. Percent sand and percent clay were derived from the STATSGO soil database [*Soil Survey Staff*, 1994]. Time-varying vegetation parameters for SiB2, such as leaf area index and roughness length, were calculated from seasonal variations of the Normalized Difference Vegetation Index (NDVI). We have used the equations and methodologies described by *Sellers et al.* [1996a, 1996b] and *Los et al.* [2000] to calculate these parameters from the 1 km global AVHRR NDVI data set described by *Teillet et al.* [2000]. The time varying parameters were then calculated. These parameters vary considerably across the domain, with vegetation parameters showing considerable heterogeneity within biome classes. Respiratory loss of carbon from the ecosystem varied with soil temperature, soil moisture, and soil texture following the parameterization of *Denning et al.* [1996]. Rather than specifying initial organic pool sizes for every grid cell in the domain, the scheme is balanced on an annual timescale, in close agreement with multiyear measurements of net ecosystem exchange (NEE) at the site [*Davis et al.*, 2003].

[14] Figure 1b shows the coarse-grid domain and outline of the three nested grids used by the coupled SiB2-RAMS model. The horizontal grid increments are 16 km, 4 km, 1 km, and 333 m, for grids 1, 2, 3, and 4, respectively. Each grid mesh has approximately 40 by 40 grid cells. There are 45 vertical levels. The vertical grid increment is approximately 20 m next to the surface and is gradually stretched to the top of the domain which is at 7.2 km. The values of the vegetation classes and SiB2 parameters at each model grid point were specified to be equal to the nearest grid point of the 1 km resolution SiB2 data set. Surface elevation was obtained from 30 second data sets supplied by the United States Geological Survey (USGS). Atmospheric fields of pressure, potential temperature, relative humidity and winds were obtained from 2.5 degree National Centers for Environmental Prediction (NCEP) reanalysis data and interpolated by the RAMS analysis package to the grid 1 mesh at six hourly intervals. The gridded data files produced were used to initialize the model and to nudge the lateral boundaries and the upper levels of the domain during the simulation. The nudging was applied to the five outermost lateral boundary points of grid 1 and to the levels above 5.5 km in all grids. Additionally, the *Klemp and Wilhelmson* [1978] radiation condition was applied at the lateral boundaries of grid 1.

[15] The water temperature of the lakes was set to 17 C based on climatological data. There is considerable uncertainty of the initial values of soil temperature and moisture. For the WLEF site, multiyear simulations driven by observed meteorology were used to specify the temperature and moisture content of the soil levels [*Baker et al.*, 2003]. For other locations the initial temperature of the soil levels were specified to deviate from the value at the first atmospheric level in accordance with the deviations at the WLEF site. The soil moisture was set to be linearly proportional to the empirical parameter b , used to relate soil moisture potential to soil wetness (see, for instance, equation (1) of *Clapp and Hornberger* [1978]), reflecting

better soil moisture retention by clay relative to that of sand. The initial volumetric water content specified using this procedure ranged from about 0.4 of saturation for sandy soils to about 0.7 of saturation for clay-like soils. The initial value of CO₂ was set to 360 ppm throughout the model domain. This value was consistent with measurements at the WLEF tower at the model initialization time. The zero-gradient lateral boundary condition was applied to CO₂ in grid 1. This assumes that the value of CO₂ at an outermost lateral grid point is equal to that of the nearest interior grid point.

5. Description of Experiments

[16] For the control simulation, cloud microphysics was not activated and the modified Smagorinsky deformation-type subgrid-scale turbulence model was employed for all the grids. The reason for choosing the control run to be cloud free was because the inclusion of cloud microphysics adds another level of complexity, and only small scattered clouds were present during the time period simulated. Also, as will be discussed, in some respects results with the inclusion of cloud microphysics did not agree well with observations. Details of the cloud parameters used for the simulation with clouds are given by *Denning et al.* [2003]. Simulations were also run to examine the sensitivity to using the Mellor-Yamada scheme on the coarser-scale grids and the Deardorff scheme on the finer-scale grids. As mentioned in section 2, neither scheme is really appropriate at an intermediate scale approximately between about 500 m and 5 km. Both grids 2 and 3 fall within this range having increments of 4 km and 1 km, respectively. Model runs were carried out using the Mellor-Yamada scheme on grids 1 and 2, and the Deardorff scheme on grids 3 and 4, and also using the Mellor-Yamada scheme on grids 1, 2, and 3, and the Deardorff scheme on grid 4. Additionally, simulations were run with cloud microphysics activated in conjunction with the turbulent kinetic energy-type sub-grid-scale parameterizations activated.

6. Results

6.1. Control Run

[17] We first evaluate the realism of the simulation by comparing grid 4 time series to observations made at the WLEF tower, then proceed to larger scales. Figure 2 shows time series of the downward short wave radiation observed at the WLEF site and model results for grid 4. Overall, the agreement is fairly good. The observed variations are evidence of clouds, which were most likely shallow cumulus. The largest reduction of short wave radiation reaching the ground occurred on 28 July, the third day of the simulation. Figures 3a and 3b show the observed and simulated potential temperature and water vapor mixing ratio, respectively, at 122 m above the surface for grid 4. The general trend of cooling and drying that occurred between $t = 40$ h and 70 h is well simulated. The peak potential temperature simulated during the first day is in good agreement with observations, but the nighttime cooling is considerably stronger than observed, particularly for the first night. The cause may be excessive low-level radiation cooling at night, particularly when the atmosphere

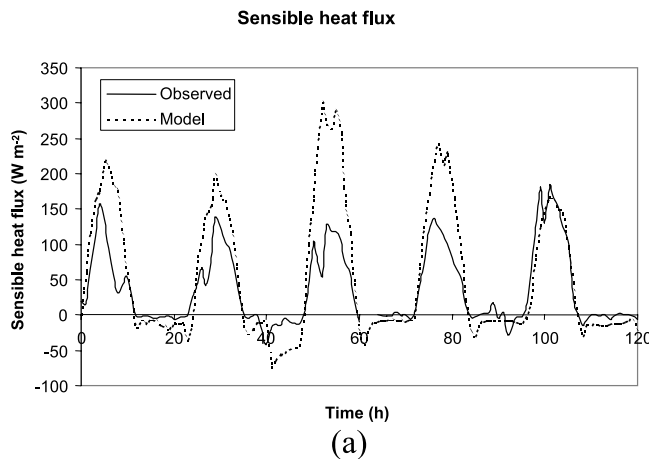
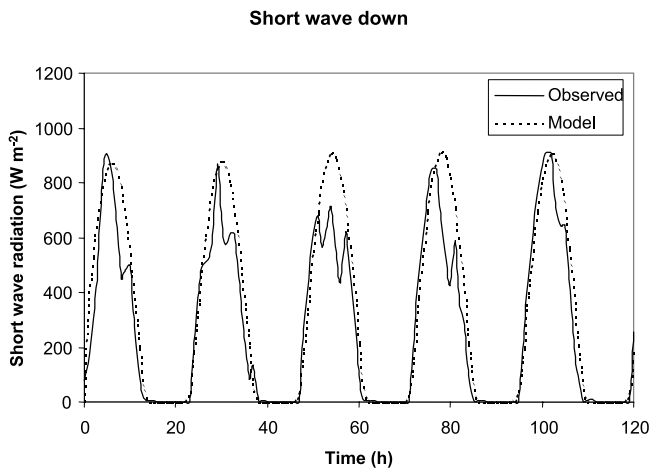


Figure 2. Observed and simulated downward solar radiation.

is very moist, although it is difficult to draw a definite conclusion from the results of this single case. Figures 4a and 4b show observed and simulated sensible and latent heat fluxes, respectively. The sensible heat flux tends to be

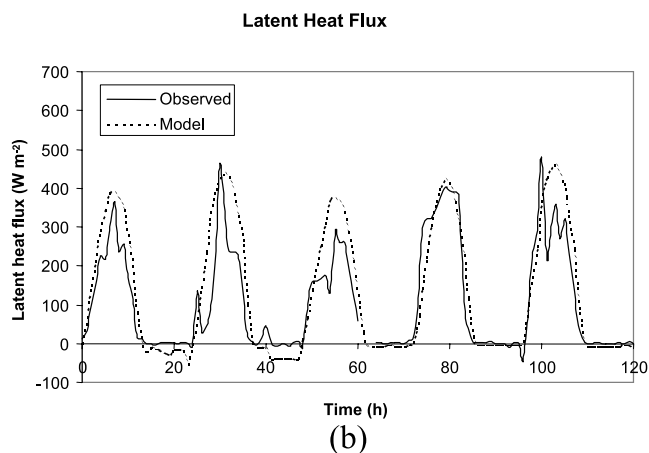
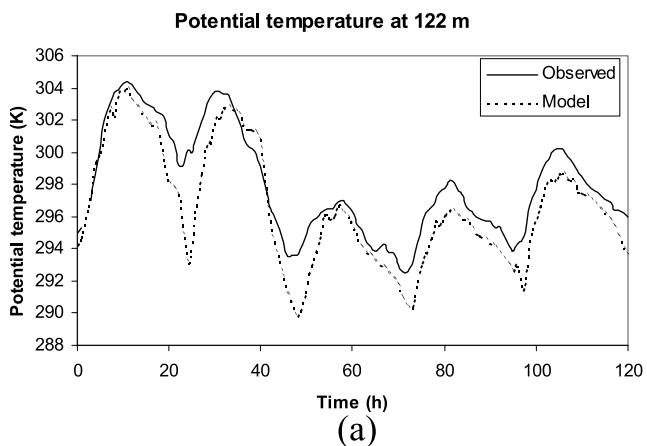


Figure 4. Observed and simulated values of (a) sensible heat flux and (b) latent heat flux at 30 m above the surface.

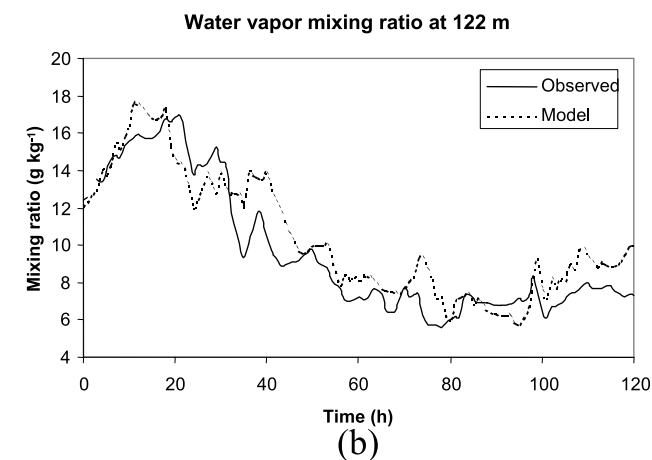
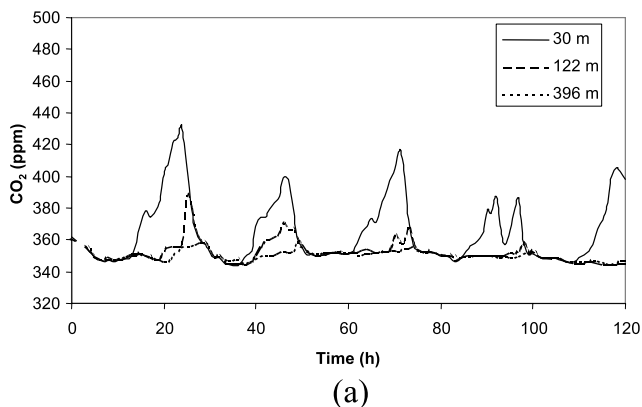


Figure 3. Observed and simulated values of (a) potential temperature and (b) water vapor mixing ratio at 122 m above the surface.

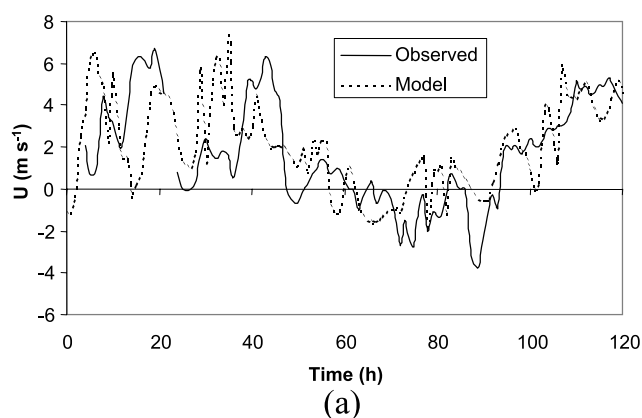
larger than observed, especially on the third day. Some of this difference is attributable to cloud cover. It should be kept in mind that the measurements do not close the energy budget, so there is some uncertainty in observed values [Davis *et al.*, 2003]. Also, this discrepancy has been analyzed in detail by Baker *et al.* [2003] who found a residual in the observations of comparable magnitude. Although the simulated potential temperature does not reach quite such high values as observed on the third day (Figure 3a), the increase in temperature from early morning values is much larger, reflecting the higher simulated sensible heat flux. Examination of the temperature difference between the surface and overlying air revealed it was at its greatest on the third day, mainly because of the excessively cold overlying air, accounting for the high sensible heat flux simulated on this day. The simulated latent heat flux agrees quite well with observations, with differences being attributable mostly to cloud cover.

[18] Figure 5 shows time series at three levels of observed CO₂ concentration at the WLEF tower and simulated results. The simulated CO₂ concentrations at 30 m tend to reach lower values during the daytime, and show higher concentrations than observed during the last three nights. Also, during the late afternoon the model usually shows a

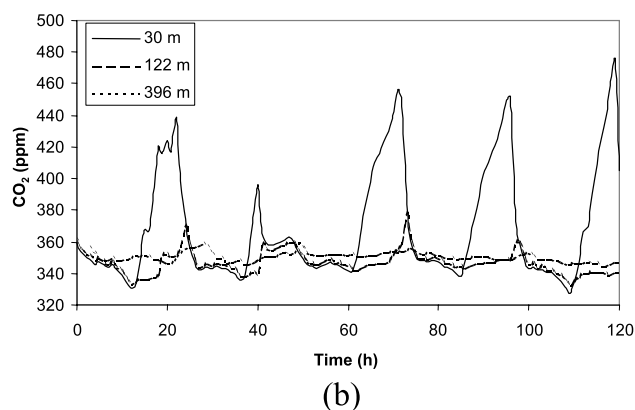
Observed carbon dioxide concentrations at three levels



x-component of velocity



Modeled carbon dioxide concentrations at three levels



y-component of velocity

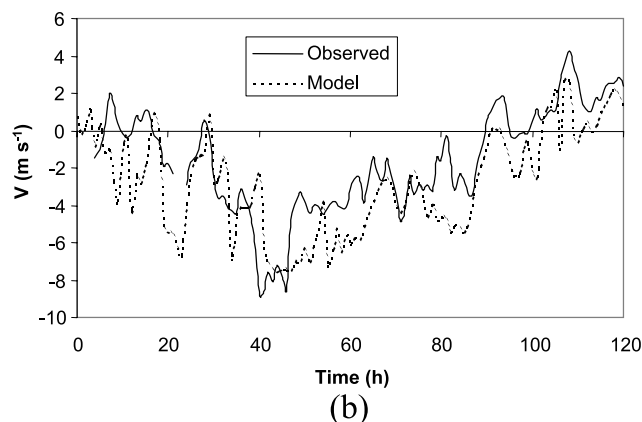


Figure 5. CO₂ concentration at three levels: (a) observed and (b) simulated.

Figure 7. Observed and simulated velocity components: (a) x component and (b) y component.

pronounced dip in concentration that is not observed. This issue was discussed by Denning *et al.* [2003] and is a result of a tendency for the SiB2 model to overestimate late afternoon photosynthetic activity. Another discrepancy is that during the daytime the simulated vertical gradient

in CO₂ is too strong, indicating that turbulent mixing is too weak. Figure 6 shows the observed and simulated CO₂ fluxes. Model results are in reasonable agreement with observations, but the simulated daytime uptake of CO₂ is slightly larger and the uptake continues later than observed in the early evening, as discussed above. Since the model overestimates NEE and underestimates vertical mixing it is not surprising that the simulated CO₂ concentration at 30 m, seen in Figure 5, is underestimated during the daytime. The reason vertical mixing is less than it should be is apparently due to a limitation of the subgrid-scale turbulence model, as will be discussed in section 6c.

Carbon dioxide flux

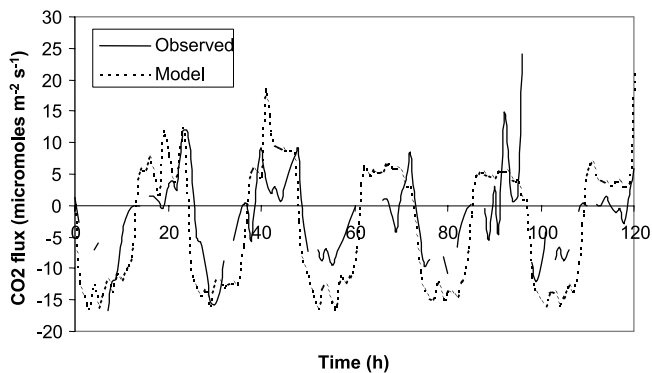


Figure 6. Observed and simulated CO₂ fluxes at 30 m above the surface.

[19] Figures 7a and 7b show observed and simulated x and y components of horizontal velocity, respectively, at 122 m above the surface. The general trends are simulated quite well. Taken together, comparisons of simulations with observations in Figures 3–7 allow confidence that advective tendencies at the WLEF site are fairly well simulated. The most significant event is the large increase of the northerly component of the flow, at $t = 40$ h (10 p.m., LST). These strong winds brought cold and dry air from the north and are the reason for the potential temperature and vapor mixing ratio drop seen in Figure 3.

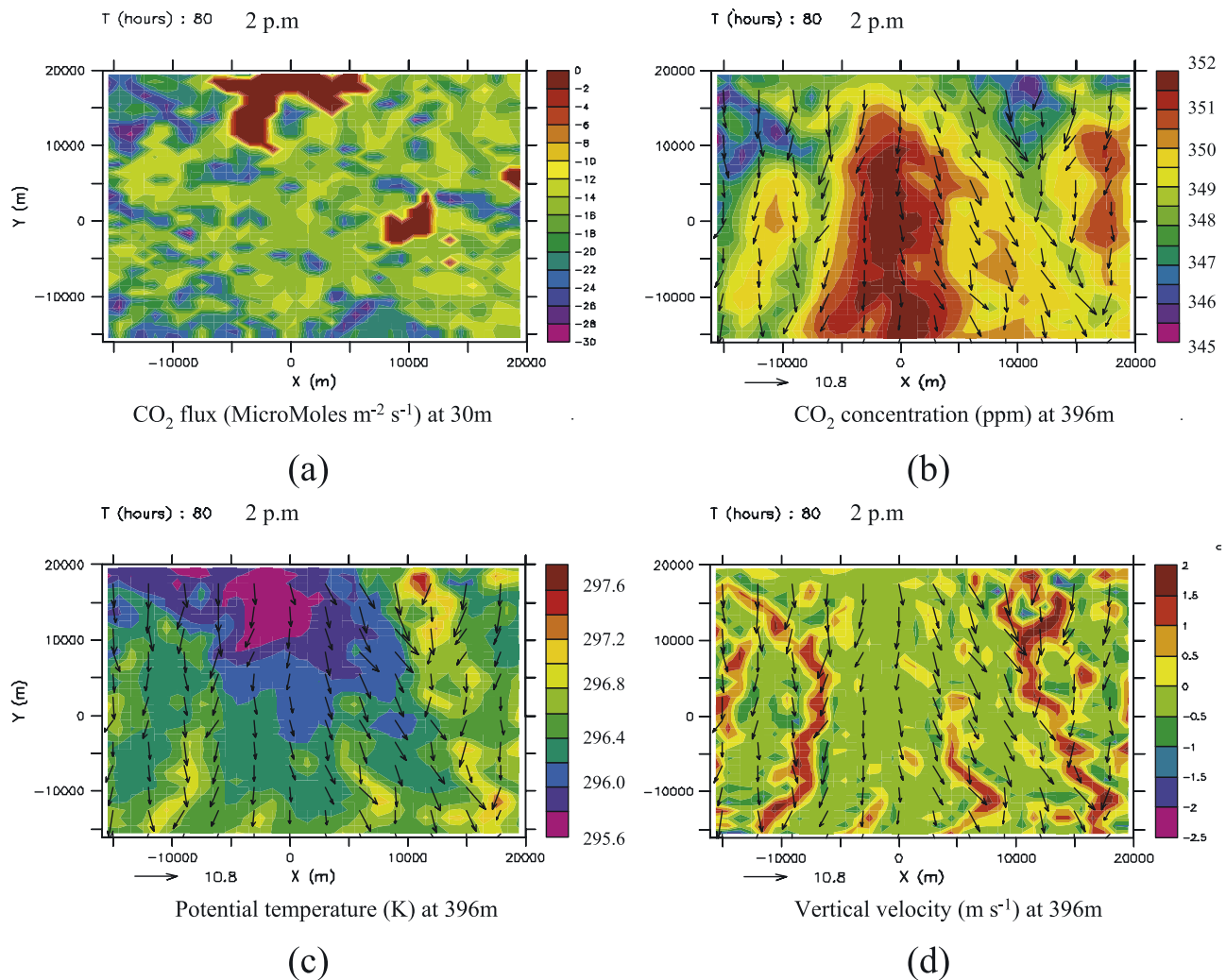


Figure 8. Horizontal cross sections of (a) CO₂ flux (micromoles m⁻² s⁻¹) at 30 m and (b) CO₂ concentration (ppm), (c) potential temperature (K), and (d) vertical velocity (m s⁻¹) at 396 m for grid 3 at t = 80 h (2 p.m. LST).

[20] Now we proceed to analyze the larger-scale variability, looking first at grid 3, which has a 1 km horizontal grid increment. Figures 8a–8d show the surface CO₂ flux at 30 m above the surface, and CO₂ concentration, potential temperature, and vertical velocity, respectively, 396 m above the surface, for grid 3, at t = 80 h (2 p.m. LST). The lakes are clearly evident in Figure 8a since the fluxes from the water are specified to be zero. There is a lake to the north of the WLEF site (the Flambeau Flowage), which is at the center of the domain, and a smaller lake to the east. At this time there is a strong draw down of CO₂ over the land. At 396 m above the surface, relatively high concentrations are advected from the northern lake, where there is no CO₂ uptake, over the WLEF site. The temperature of the air above the lake is considerably cooler than that over the land, which has warmed due to strong sensible heat fluxes. This colder air advects southward and slowly sinks bringing down higher values of CO₂ from aloft, which contributes to the CO₂ anomaly at this level. At the same time air is lifted on the margins of the cold sinking air, leading to narrow lines of upward motion.

The upward motion lifts air depleted in CO₂ from nearer the surface. To a lesser extent the smaller lake to the east has a similar effect. The contrast in CO₂ concentration between high and low values at this level, is 6 ppm, which is quite high for this relatively small area. The depth of the CO₂ anomaly caused by the northern lake extends throughout the depth of the boundary layer (not shown). These results are similar, in some respects, to observations of CO₂ concentrations at midday for Candle Lake during the Boreal Ecosystem-Atmosphere Study (BOREAS), reported by *Sun et al.* [1998]. They found higher concentrations of CO₂ over the lake than at the same level over land, which they suggest are caused by downward motion induced by the lake breeze. In this modeling study, a lake breeze is evident in the early morning and similarly higher concentrations occur over the lake. However, an unexpected feature of this simulation is that the impact of the subsiding air on CO₂ concentrations extends well downstream of the lake. This result suggests that considerable variability at the WLEF site could be caused by circulations induced by nearby lakes.

[21] The simulated variations of order 5 ppm due to fine-scale meteorological fluctuations forced by small lakes is intriguing and has important implications for the interpretation of observed time series through transport inversion. Quantitative flux estimation in the face of such fluctuations requires very high resolution such as used here, which would be computationally prohibitive in continental-scale analysis or even over a limited area for periods of months or years. In coarser mesoscale or global models, such variations cannot be modeled and must therefore be treated as representativeness error [Engelen *et al.*, 2002].

[22] We now move on to analyze the larger regional-scale variability, looking at results for grid 1, which has a horizontal grid increment of 16 km. The contrast between the large-scale flow field at the start of the simulation and at the time of the cold air mass intrusion from the north is illustrated in Figures 9a and 9b, which show simulated potential temperature and wind vectors, at $t = 4$ h and 44 h, respectively, at approximately 100 m above the surface, for grid 1. Early on, there were predominantly west to southwesterly winds over most of the domain. At $t = 44$ h the winds have a strong northerly component and cold air is being advected southward across the location of the WLEF tower. Also, seen in Figure 9a are lake breezes, which are particularly evident for Lake Superior.

[23] Figures 10a and 10b show horizontal cross sections of the CO_2 flux at $t = 90$ h (midnight) and at $t = 102$ h (noon), respectively, for grid 1. During the night there is stronger respiration to the south. This is highly correlated with temperature, which tends to be warmer to the south. The soil tends to be more moist to the south as well, which would also encourage respiration, although this was not as significant a factor as the temperature. During the daytime the strongest uptake of CO_2 is focused near the center of the domain and to the east of the WLEF site. This strong uptake occurs for the deciduous broadleaf vegetation class (see Figure 1a). Sensitivity tests indicated that the reason uptake is less for the mixed forest in this region is mainly due to the onset of high-temperature stress, which occurs at slightly cooler temperatures in mixed forest than in broadleaf. The daytime canopy temperatures reach fairly high values on this day (see Figure 3a at $t = 102$ h) causing the mixed forest to be stressed and the simulated photosynthetic rate to be less than for the deciduous broadleaf trees. Further south, higher canopy temperatures inhibit photosynthesis in regions classified as deciduous broadleaf to some extent as well and, coupled with higher respiration rates, results in less net CO_2 uptake.

[24] We next look at simulated spatial patterns of regional-scale CO_2 variability that occurred at low levels. Figure 11 shows horizontal cross sections of CO_2 concentration at various times, at about 100 m above the surface. Before sunrise, at $t = 94$ h (4 a.m. LST) there is a region of low CO_2 concentrations surrounded by a ring of higher concentrations. By $t = 100$ h (10 a.m. LST), this ring has started to disappear due to the onset of vertical mixing and photosynthetic uptake of CO_2 . By $t = 104$ h (2 p.m. LST) CO_2 concentration has fallen considerably over land. Higher concentrations of CO_2 over the lakes are apparent. By $t = 118$ h (4 a.m. LST) there are low concentrations of CO_2 in the center of the domain, although the ring-like structure of higher concentrations that occurred the night before is not

so well defined. The reason for the unusual pattern observed at $t = 94$ h is made apparent by Figures 12a, 12b, and 12c, which show the vertical velocity field at about 100 m, the topography and wind vectors at about 50 m, and the surface temperature, respectively, at $t = 90$ h (midnight). The ring of upward motion is the cause of the high CO_2 concentrations seen in Figure 11 (4 a.m. plot). As can be seen from the topography and wind vectors, the airflow is divergent over the plateau near the center of the domain and is convergent in the valleys and over the lakes where the upward motion occurs. This flow is a weak katabatic wind caused by nighttime cooling of near surface air over higher elevations. It is more apparent at $t = 94$ h than the following night at $t = 118$ h, because the environmental winds were lighter. The stronger respiration to the south shown in Figure 10a, also plays a role in producing high southerly CO_2 concentrations during the early morning at 100 m. Variations in respiration flux are driven primarily by variations in soil temperature (Figure 12c). Since the ring of upward motion occurs near the boundaries of the domain, we also ran a simulation with a much larger domain. The effect was weakened, but still significant. The effect is a shallow phenomenon and does not extend much above 100 m from the surface. Nevertheless, it represents quite a significant low level advection of CO_2 from some regions to others, which may need to be taken into account in observational studies if accurate CO_2 budgets are to be achieved. These results are consistent with studies by Hollinger *et al.* [1994] and Lee [1998], which suggest that cold air drainage flows could play a significant role in transporting CO_2 . Observational evidence of the importance of cold air drainage for nocturnal budgets is provided by the results of Lavigne *et al.* [1997] and Jarvis *et al.* [1997]. They found that when vertical mixing is small the sum of the storage and eddy correlation turbulent flux of CO_2 estimates were much smaller than the estimated respiration. The simulation presented here indicate that density-driven drainage flows over even fairly simple regional topography may play an important role in horizontal redistribution of CO_2 , and pose challenges for quantitative flux estimation by inverse modeling.

[25] Figure 13 shows x/z (east–west) and y/z (north–south) cross sections of CO_2 concentrations at $t = 90$ h (midnight) and $t = 102$ h (noon), for grid 1 (see Figure 1 for location of transects). The x/z cross section is in the southerly part of the domain at $y = -220$ km and intersects Lake Michigan. The y/z cross section is in the easterly part of the domain at $x = 180$ km and intersects Lake Superior. At midnight the x/z cross section shows a shallow layer with high concentrations of CO_2 has developed over land due to respiration. Above this shallow layer there is a deeper residual layer with reduced CO_2 concentrations, caused by daytime photosynthetic activity, extending to a height of approximately 1.7 km. At this height there is a strong positive vertical gradient of CO_2 between the residual boundary layer and the free troposphere. At noon the x/z cross section shows lowest CO_2 concentrations near the surface, particularly to the west. This is consistent with Figure 10b, which shows a relatively strong uptake in the southwest region of the domain at this time. Over Lake Michigan, the CO_2 concentrations near the surface are considerably higher than over land, and also higher than over the lake at midnight. At midnight the y/z cross section

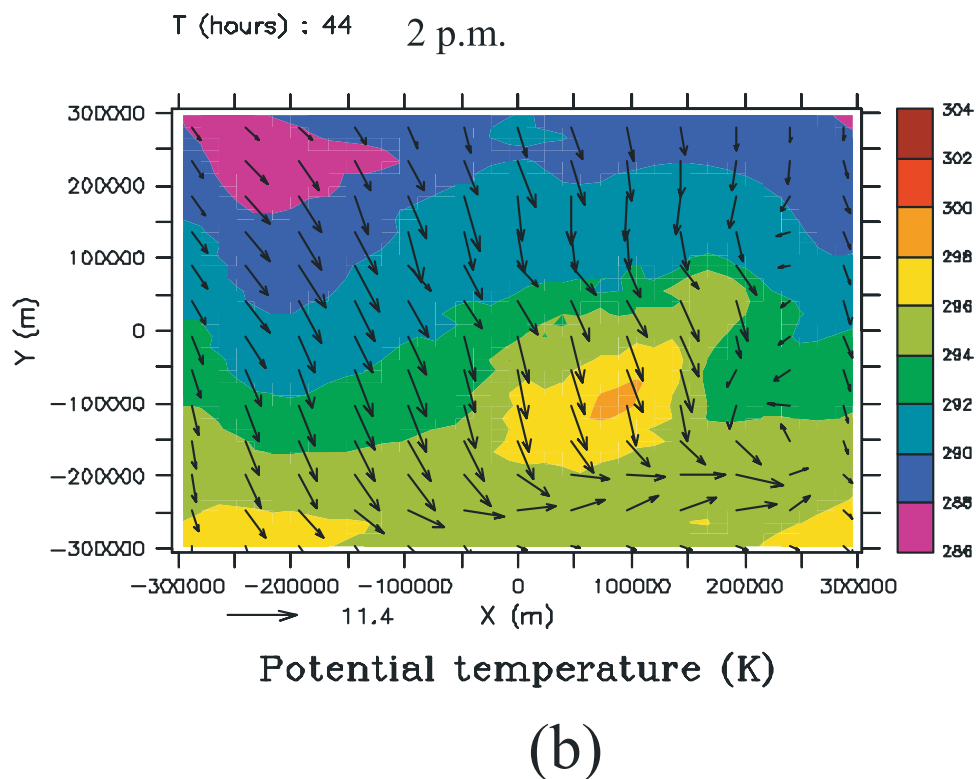
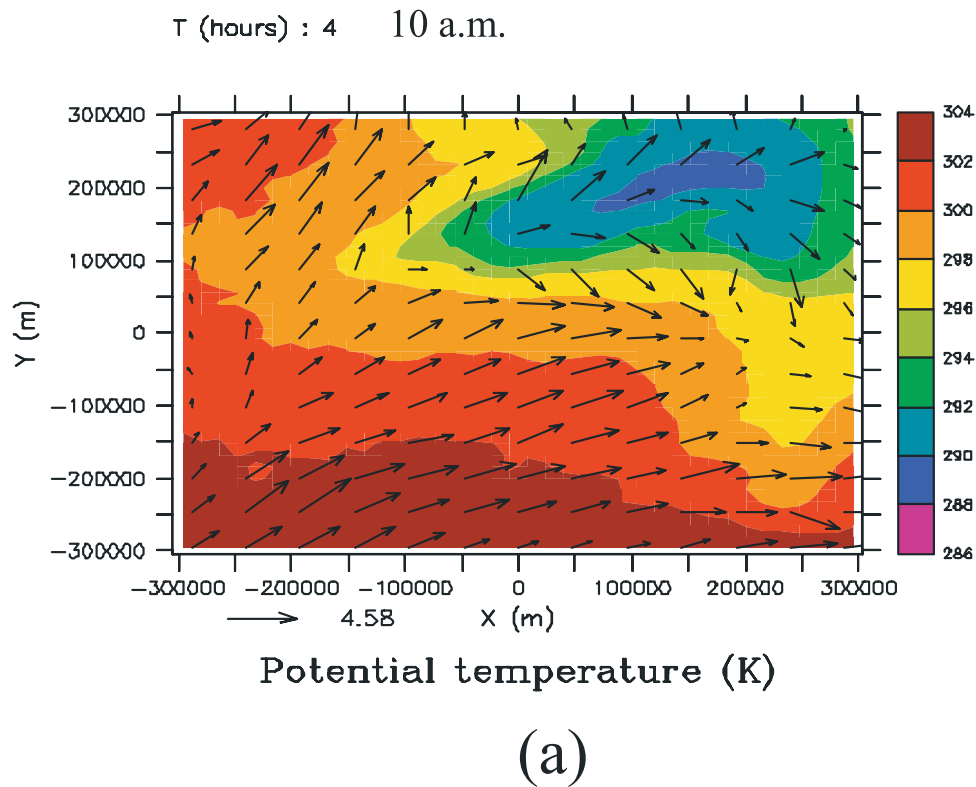
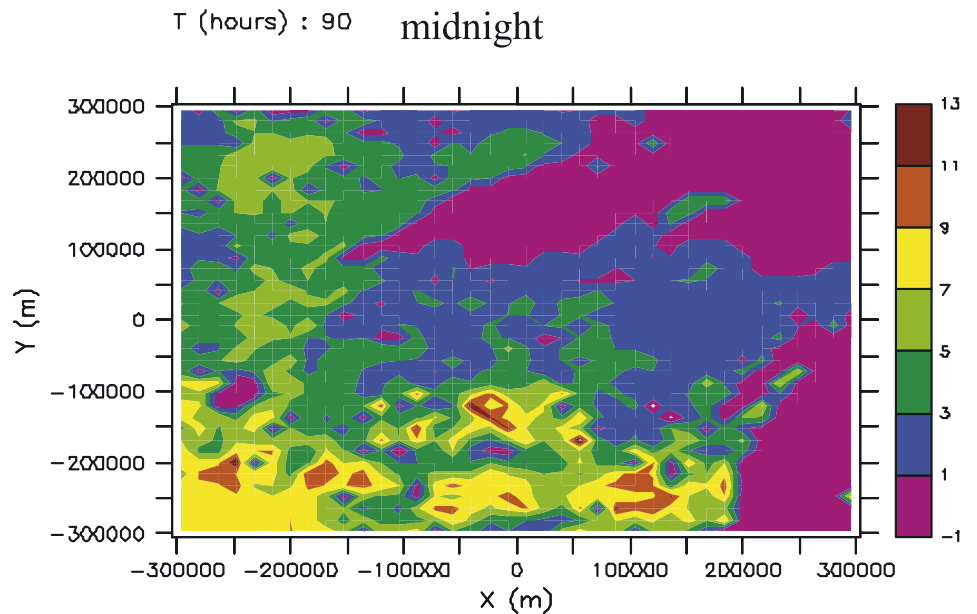


Figure 9. Horizontal cross section of simulated potential temperature (K) and wind vectors for grid 1, at approximately 100 m above the surface: (a) 4 h and (b) 44 h.

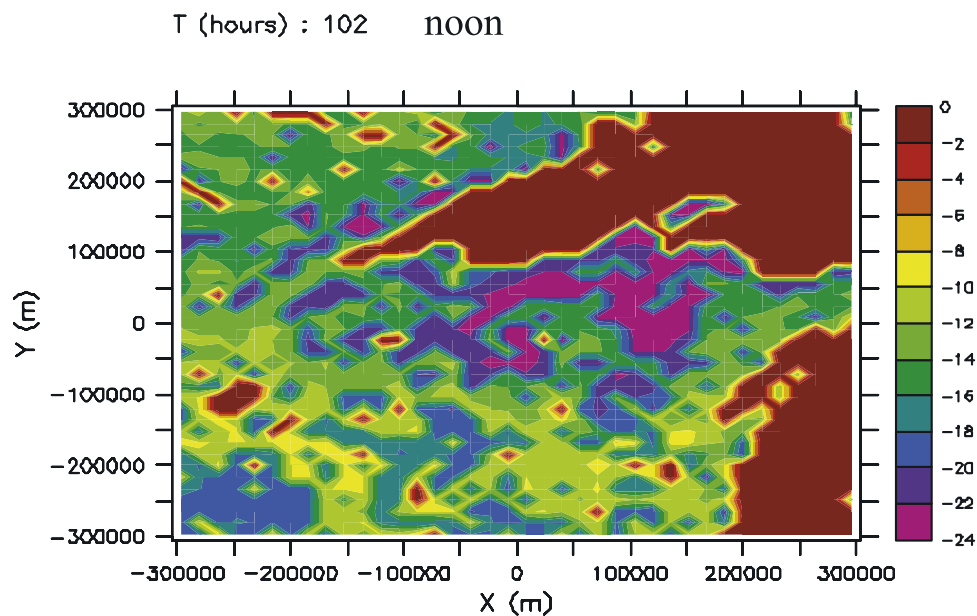
shows high concentrations of CO_2 near the surface over the land with a minimum occurring at $z = 300$ m between $y = -100$ km and $y = 0$ km. There is a region of strong daytime uptake centered slightly to the north of this minimum as is

evidenced by the low concentrations near the surface at noon and the large negative surface fluxes at this location seen in Figure 10b. Over Lake Superior the concentrations near the surface are high at noon, but at midnight are very low.



CO₂ flux (MicroMoles m⁻² s⁻¹) at 30m

(a)



CO₂ flux (MicroMoles m⁻² s⁻¹) at 30m

(b)

Figure 10. Horizontal cross section of the simulated CO₂ flux (micromoles m⁻² s⁻¹) at the first model level above the surface for grid 1: (a) 90 h (midnight) and (b) 102 h (noon).

[26] The diurnal cycle of CO₂ concentrations over the lakes is not locally forced (surface CO₂ fluxes over water are prescribed to be zero at all times). This is further examined in Figures 14a and 14b, which show time series of CO₂ concentrations and vertical velocity, respectively,

averaged for a 80 km by 80 km square area over Lake Superior, at $z = 255$ m. The averaging area is centered at $x = 0$ km, $y = 140$ km and was chosen to be as far away from the domain boundaries as possible. Figure 14a shows a strong diurnal cycle of CO₂ concentration occurring over

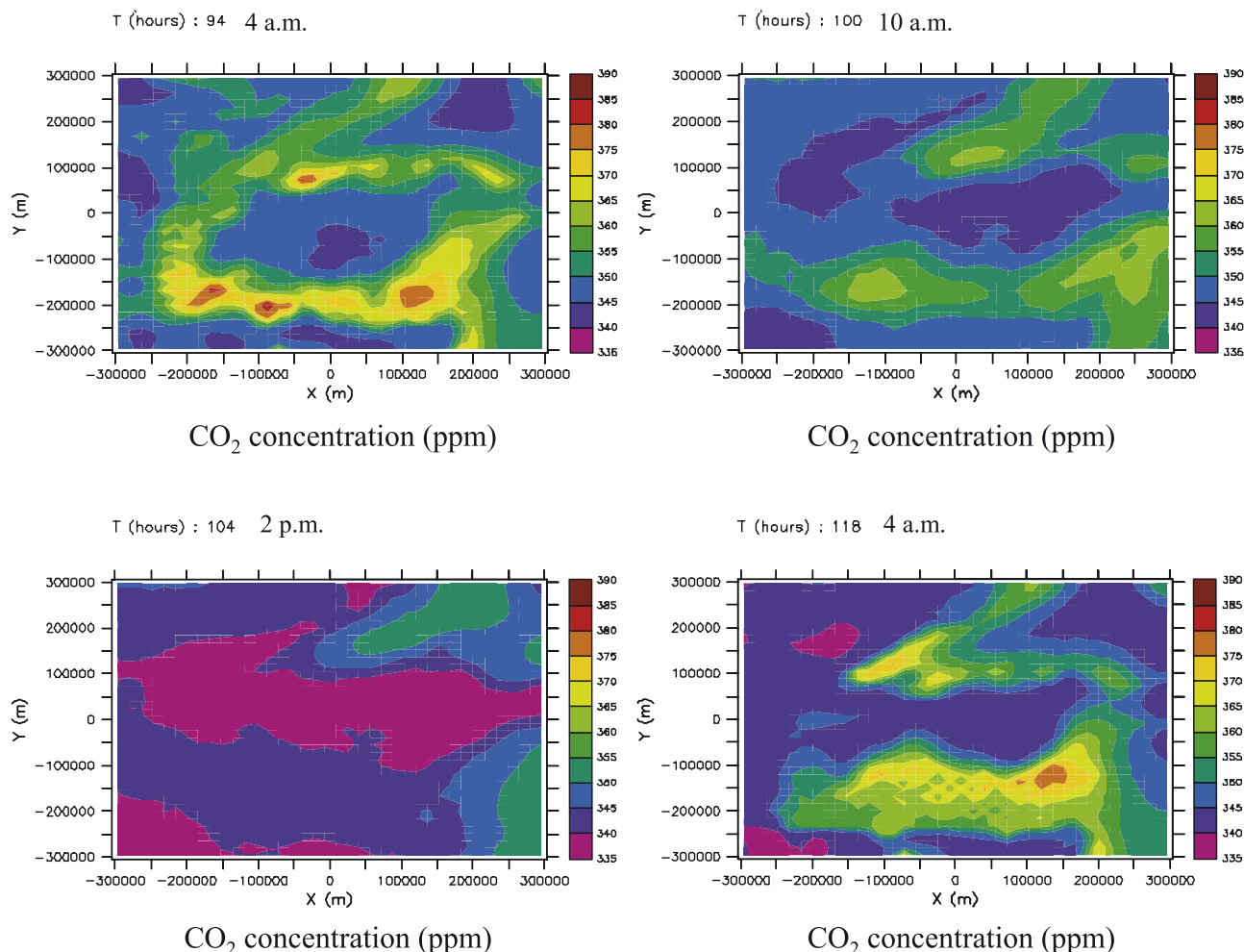


Figure 11. Horizontal cross sections of CO₂ concentration (ppm) at various times at approximately 100 m above the surface for grid 1.

Lake Superior of approximately 10 ppm. The minimum occurs at or just before midnight and the maximum occurs 6–9 hours later, soon after daybreak. The vertical velocity field also shows a pronounced diurnal cycle with a minimum occurring at noon or slightly after, and a maximum occurring approximately at midnight. It can be seen that decreasing (increasing) CO₂ concentrations tend to be correlated with downward (upward) motion. Notice that the mean vertical motion during this time period is downward over the lake, and that the duration of the downward motion tends to be longer than the duration of upward motion. Further examination of the model fields indicate that the large decrease in CO₂ concentration that occurs during the first day is due to air which is depleted in CO₂ over land, and which is vertically mixed within the turbulent boundary layer, being advected over Lake Superior and then subsiding to low levels. This advection is due to the ambient westerly flow and also to the return flow of the lake breeze that occurs above the onshore flow (Figure 9a). Air depleted in CO₂ can be lifted up at the lake breeze front during the daytime and then advected over the lakes in its return flow. Subsidence over the lake is expected since when the lake breezes develop the low-level flow over the lakes is divergent, as

can be seen in Figure 9a. These results are consistent with a study of the dispersion of pollutants from industrial sources over Lake Michigan using RAMS and a Lagrangian Particle Dispersion Model [Nicholls *et al.*, 1995]. It was found that both the ambient winds and the return flow of the lake breeze played a significant role in advecting particles across Lake Michigan. Interestingly, during the evening when the katabatic winds first develop in this study they bring air with very low concentrations of CO₂, produced by daytime photosynthetic activity over land, onto Lake Superior. This is why the minimum tends to occur quite late in the evening and sometimes as late as midnight. This effect is particularly prominent for Lake Superior since the slope of the terrain to the west of Lake Superior is relatively steep, resulting in strong down slope winds during the night (Figures 12a and 12b), and also because there is a large daytime uptake in this region (Figure 10b). Later on in the night as respiration over land increases low level CO₂ concentrations, the katabatic winds cause air rich in CO₂ to be advected to the coastal regions, as can be seen in Figure 11 at $t = 94$ h and 118 h (4 a.m.).

[27] The advection of CO₂ across the lakes at low levels is also enhanced at night by the ambient winds since the

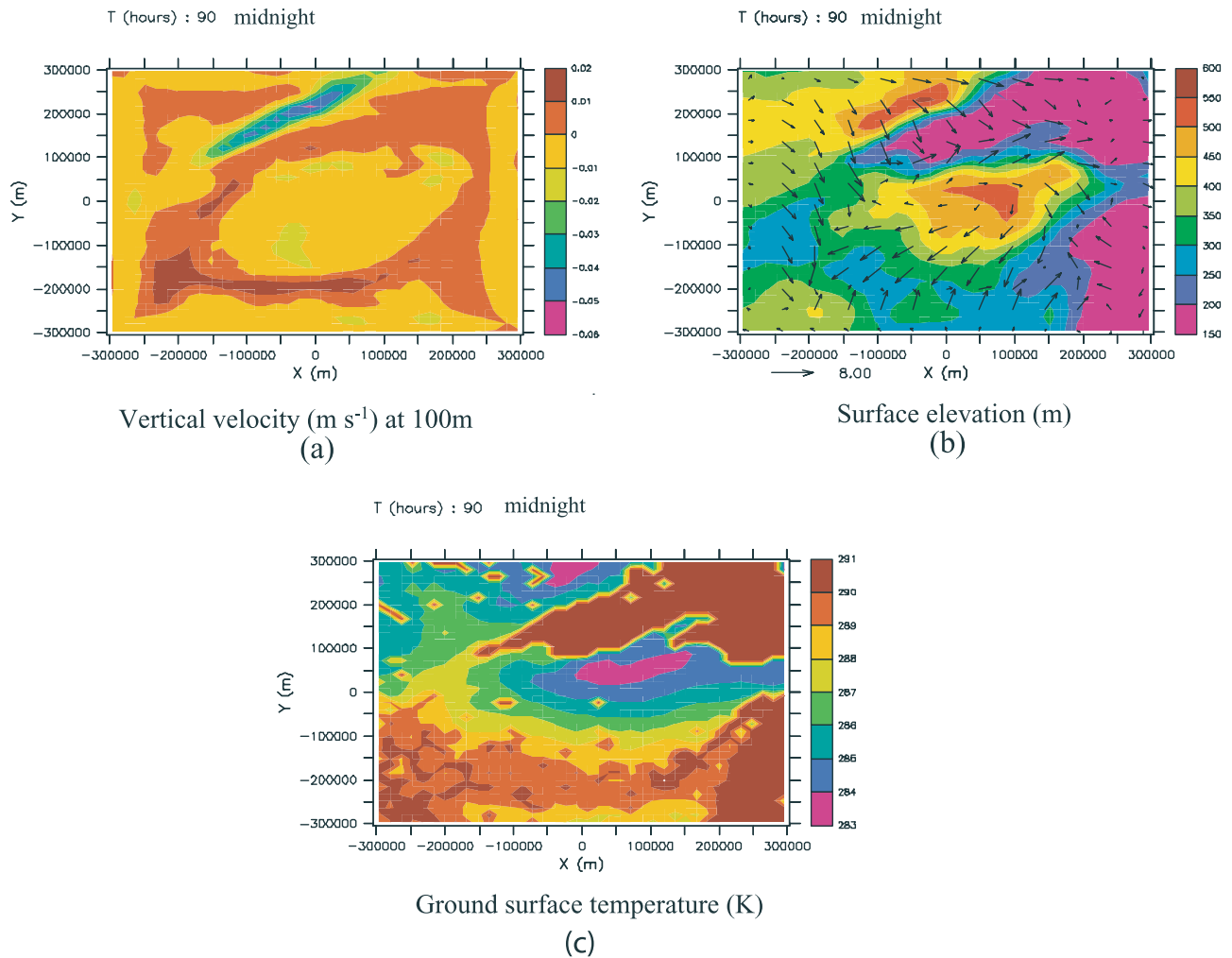


Figure 12. Horizontal cross sections of (a) vertical velocity (m s^{-1}) at approximately 100 m above the surface, (b) surface elevation (m) and wind vectors at 50 m, and (c) surface temperature (K) at 90 h (midnight) for grid 1.

lake breeze circulation has ceased and no longer impedes the flow. It is also possible that a land breeze circulation enhances the offshore flow. However, it is difficult without further sensitivity tests to gauge how important this effect is and to clearly distinguish it from the katabatic winds, since the temperature over land is very much dependent on its elevation. These mechanisms account for the peak CO_2 concentrations over the lake occurring around day break. At this time the CO_2 concentration decreases with height above the lake reaching a minimum a few hundred meters above the surface. This is because boundary layer air depleted in CO_2 over land during the previous day has advected over the lake as well. Subsidence of this air during the daytime also contributes to CO_2 concentrations over the lake decreasing with time at low levels.

6.2. Simulation With Clouds

[28] The simulation with cloud microphysics activated produced early morning fog on the second and third days, apparently related to the excessive nighttime cooling that occurred and because the atmosphere was moist. This resulted in the heat fluxes being delayed in the early

morning until the fog had dissipated. There was no indication of fog in the observations on these days. Scattered shallow cumulus clouds occurred during the simulation, but they were not as prevalent as actually occurred.

[29] Figure 15 shows a vertical cross section of CO_2 concentration, wind vectors, and cloud water for grid 4 at $t = 107$ h (5 p.m. LST). The cross section intersects shallow cumulus clouds at the top of the mixed layer. The peak magnitude of the liquid water mixing ratio in the largest cloud is 1.8 g/kg. The cloud updraft velocity is 2–3 m/s. This updraft has lifted air depleted in CO_2 resulting in an approximately 4 ppm difference in concentration between the cloud free air at the upper levels of the boundary layer. Also evident are small-scale turbulent boundary layer eddies which are resolved by the fine-scale grid.

[30] The variance of CO_2 in the presence of these small cumulus clouds tended to be larger than when clouds were not present, particularly near the top of the boundary layer. However, even in the absence of clouds, large turbulent eddies often produced variations of CO_2 concentrations as large as 2–3 ppm. These variations of CO_2 concentrations within the turbulent boundary layer can be considered to be

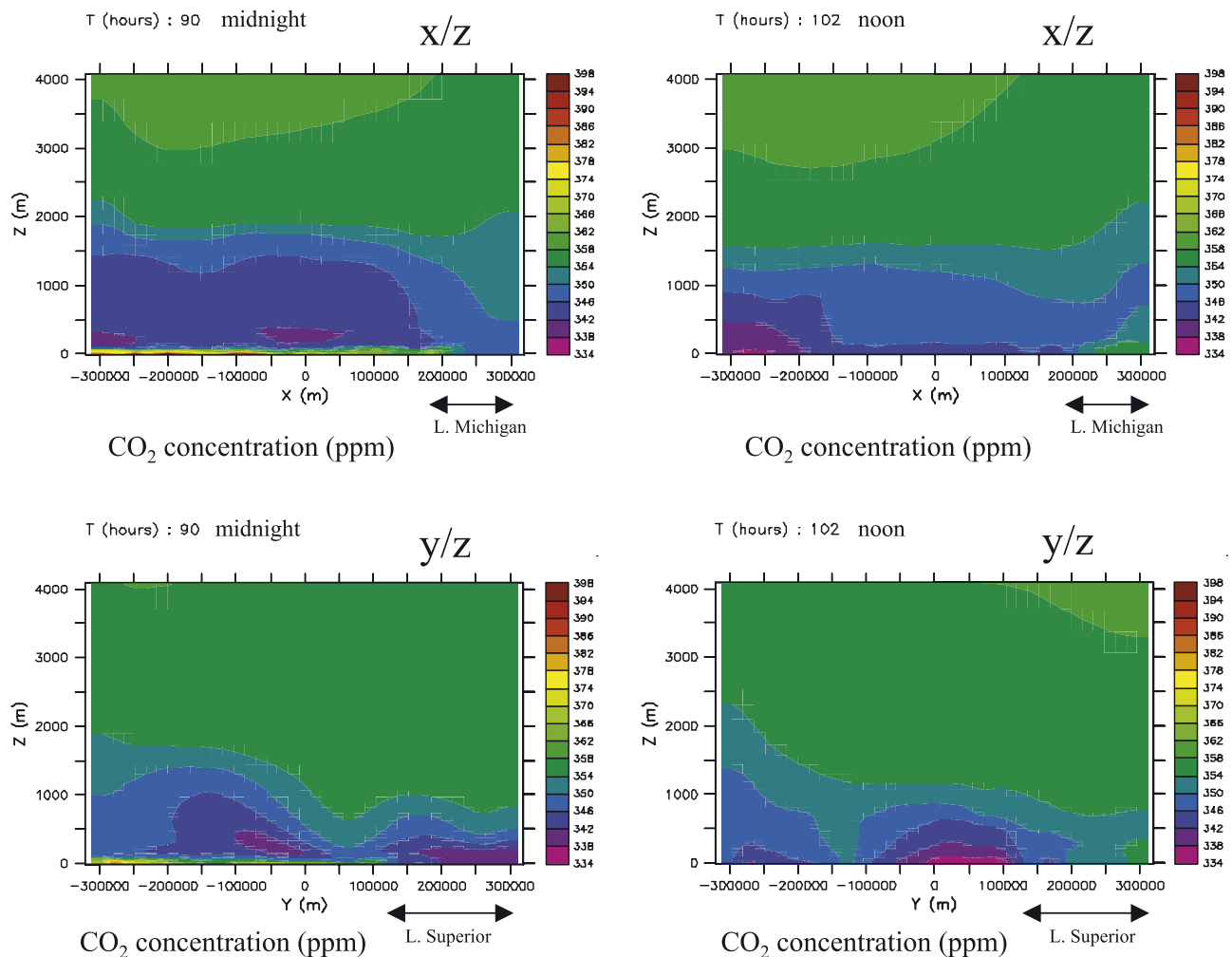


Figure 13. The x/z (east–west) and y/z (north–south) cross sections of CO_2 concentrations at $t = 90$ h (midnight) and $t = 102$ h (noon) for grid 1.

“noise” as far as measurements are concerned, since they are only indirectly related to surface forcing.

6.3. Sensitivity to TKE Parameterizations

[31] It was found that using the Deardorff scheme on grid 3 produced considerable numerical noise (alternating pattern of large variations with a scale of two grid cells) compared to the simulation that used the Mellor-Yamada scheme on grid 3. The Deardorff scheme is designed for large eddy simulations, so this result is not too surprising. The Mellor-Yamada option in RAMS uses the deformation scheme for horizontal diffusion (section 2), the same as for the control run, which is probably why it works better on grid 3. Figure 16 shows results for the CO_2 concentrations at three levels for this latter case, which used the Deardorff scheme only on grid 4 and the Mellor-Yamada scheme for the other grids. Comparing to Figure 5 it can be seen that this simulation is an improvement in some respects over the control simulation. The concentrations at the 30 m level compare more favorably with the observations on the last three nights. Furthermore, the curves during the daytime lie almost on top of one another, as observed. These improvements are because of a higher degree of vertical mixing for

this simulation. Further examination of the model output revealed that the lower values on the last three nights compared to the control simulation are due to larger vertical mixing between the lowest model levels, mainly beneath level 100 m. During the daytime there was greater vertical mixing, as well, particularly by small eddies, which led to more homogeneous boundary layer concentrations. However, the fields were not as smooth as for the control case with some numerical noise evident at times. This was a particular problem when this sub grid scheme was used with cloud microphysics activated. Also, the late afternoon dip in CO_2 concentration at 30 m tends to be larger than for the control run.

[32] During the second night the simulated CO_2 peak at 30 m in Figure 16 is not very large and shows a relative minimum occurring at $t = 43$ h. This also was the case for the control simulation, shown in Figure 5, and occurred for two reasons: The first is indicated by Figure 17, which shows vertical profiles of CO_2 , potential temperature and the y component of velocity near the surface, at $t = 40$ h and 43 h. The high concentration CO_2 air near the surface at $t = 40$ h is replaced by air advected from the north and which is vertically mixed through a depth of approximately 200 m,

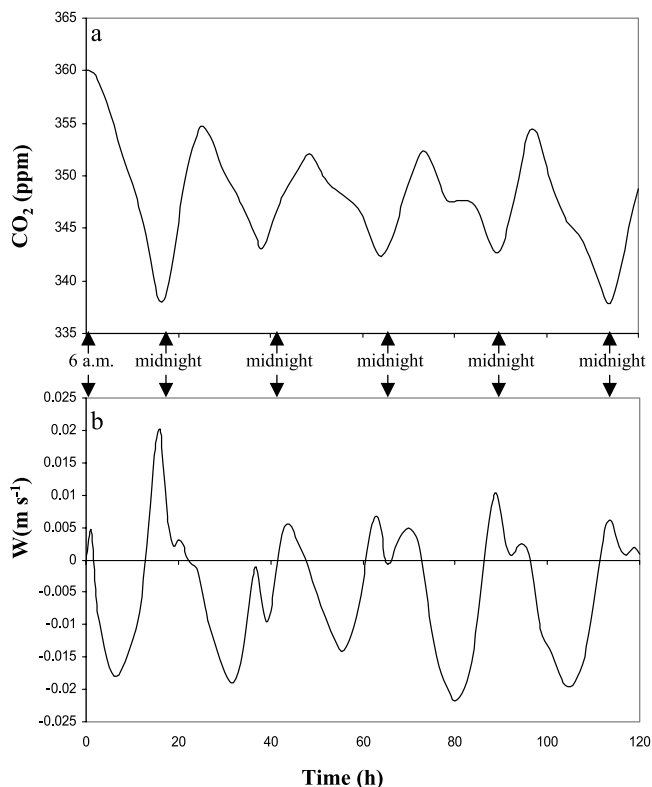


Figure 14. Time series of (a) CO_2 concentration (ppm) and (b) vertical velocity at 255 m averaged for a 80 km by 80 km area over Lake Superior.

resulting in reduced concentrations near the surface at $t = 43$ h. This transition to a mixed layer structure is also evident in the vertical profile of potential temperature. The reason why the cold air advected from the north is mixed through a 200 m depth is suggested by the y component of the wind, which shows considerable strengthening of the low level wind shear between $t = 40$ h and 43 h. Therefore it is very likely that the vertical mixing is due to shear production of TKE. The second reason is because of the small lake to the north of the WLEF site. During the night, there is no respiration occurring over the lake, unlike on the land, so the concentration remains at relatively low values. The intrusion of air from the north caused the relatively low values from the lake to be advected over the WLEF location. This effect is sensitive to the wind direction, so it may not have actually occurred on this night because the simulated wind direction did not agree exactly with observations.

[33] The increased vertical mixing due to shear production on the second night was mainly resolved by the fine-scale grid, which showed more updrafts and downdrafts at $t = 43$ h than at $t = 40$ h (not shown). This effect was also evident for simulations with just grid 1 activated, but in this case the subgrid-scale parameterization was responsible for the increased vertical mixing. For the deformation scheme this was due to the dependence of the mixing coefficients on the Richardson number, and for the Mellor-Yamada scheme to the shear production term in the prognostic TKE equation. On the other hand, the effects of the small lakes, which

were not resolved by the large-scale grid, were not accounted for, so the CO_2 concentration at 30 m, while less than on the other nights, did not show a relative minimum at $t = 43$. Therefore longer duration regional simulations, which will use much larger grid increments than the 333 m used on grid 4 in this study, should be able to represent the effects of large-scale vertical wind shear on CO_2 variability reasonably accurately, but the effects of small lakes will of course be unresolved.

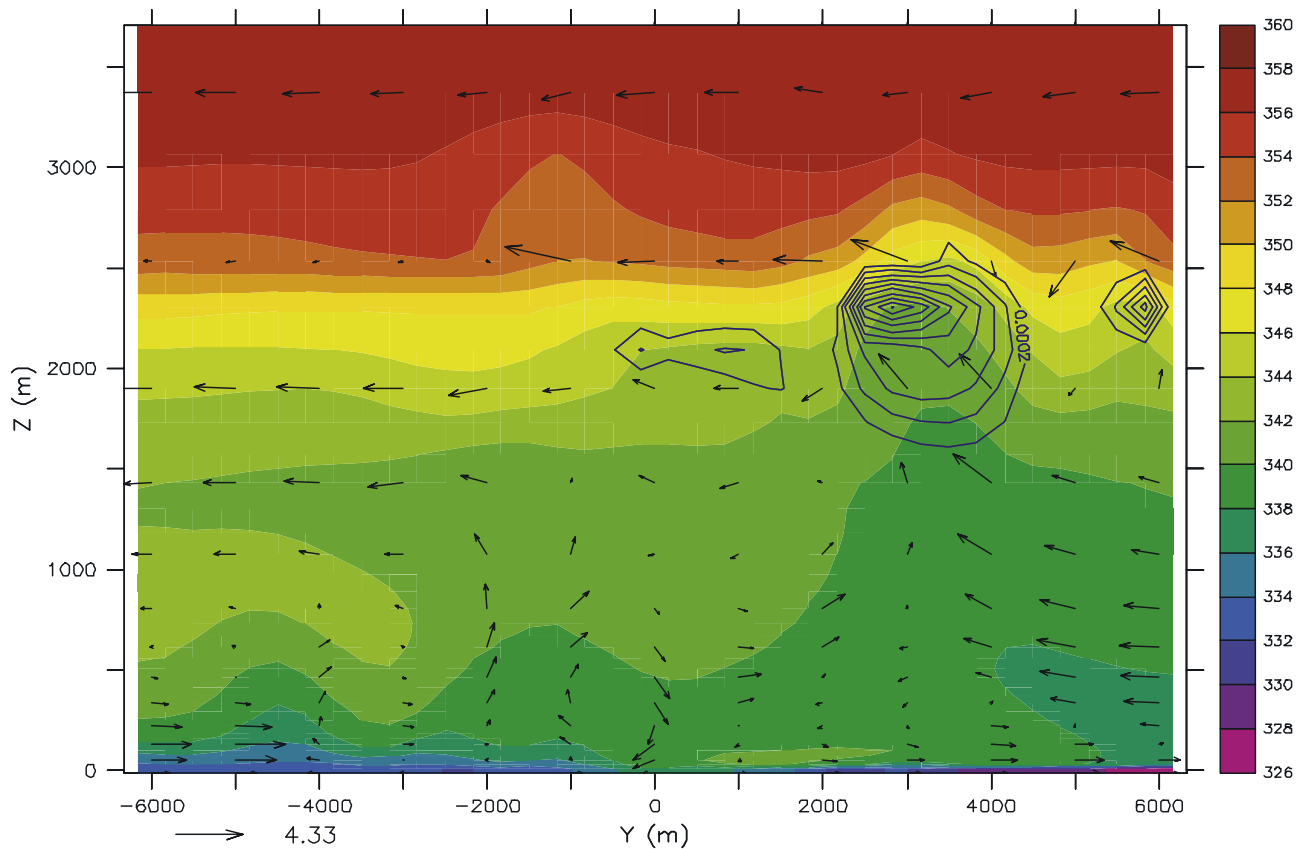
[34] In summary, these sensitivity tests did not reveal significant differences between the modified Smagorinsky scheme used in RAMS and the Mellor-Yamada scheme for regional scales. There were both advantages and disadvantages of the Deardorff TKE scheme compared to the modified Smagorinsky scheme for small scales.

7. Conclusions and Discussion

[35] We have tested the ability of a coupled biosphere-atmospheric model to simulate observed quantities at a tall tower site and identified some of the processes causing CO_2 variability. The overall agreement between model results and observations made at the WLEF site is encouraging. One discrepancy was that there was more low level cooling than observed during the first two nights. This may be due to excessive radiational cooling when the atmosphere is very moist, but it is difficult to draw any definite conclusion from the results of this one simulation. Another discrepancy was that late afternoon uptake of CO_2 was larger than observed, as has also been noted by *Denning et al.* [2003] and *Baker et al.* [2003].

[36] In addition to the diurnal cycle of CO_2 fluxes from vegetation and surface vegetation heterogeneity causing CO_2 variations at the WLEF site, this simulation demonstrated variability brought about by small lakes, vertical wind shear, boundary layer thermals and clouds. These factors introduce meteorological “noise” to the signal that is measured at the site. Particularly noticeable is that results suggest that small lakes near the WLEF tower could have significant local impacts on CO_2 concentrations, both during the day and at night that are unrelated to the surface flux. The effects of the lakes was not just caused by the absence of surface CO_2 fluxes, but also due to vertical motions brought about by the temperature contrast between the lakes and the ground and the resulting large difference in surface heat flux. This suggests that interpretations of concentration anomalies at the WLEF site should be made with caution, as they can be produced by purely physical advective effects on the scale of 10 km or so. There were also significant CO_2 variations caused by turbulence induced by vertical wind shear when there was a cold air intrusion from the north during the night on 27 July and the winds picked up in strength. Quantitative flux estimation from continuous measurements at continental sites will probably require either accurate and very high resolution transport models or the proper treatment of representation error that arises from meteorological effects.

[37] The simulation showed considerable regional scale variability in CO_2 concentrations. Generally, there was more respiration in the southern part of the domain due predominantly to warmer temperatures, so the average uptake of CO_2 over the course of the simulation was less in the south



CO₂ concentration (ppm) and cloud contours

Figure 15. The y/z cross section of CO₂ concentration (ppm), wind vectors, and contours of cloud water mixing ratio (kg kg⁻¹), at 107 h (5 p.m. LST) for grid 4.

than in the center of the domain. Particularly strong uptake occurred for the deciduous broadleaf class, due to greater tolerance of high canopy temperatures. At night, katabatic winds caused convergence and low level upward motion in the valleys and at the lake shores, which lifted high CO₂ concentration air aloft, leading to regional-scale nonbiological variability. Concentrations of CO₂ were relatively high over the Great Lakes during the daytime and were relatively low during the night near the surface, compared to values over land, due to the absence of CO₂ fluxes over the lakes. Nevertheless, in spite of the absence of CO₂ fluxes the model showed a significant diurnal oscillation of CO₂ concentration over the Great Lakes, which was particularly strong over the western part of Lake Superior. Katabatic winds, the ambient winds and the return flow of the lake breeze all played significant roles in causing this oscillation. This result suggests that there is a significant amount of CO₂ transferred off the lakes during the daytime and early on in the night, and onto the lakes later on in the night. This oscillation was of course not as strong as the diurnal cycle over land, which is why CO₂ concentrations are relatively high (low) in the daytime (at night) over the lakes compared to over land. Nevertheless, the oscillation is still relatively large and there must be significant advective effects influencing CO₂ concentrations over land in the coastal regions, particularly downstream of the lakes. These large-scale advective effects could be important terms in the CO₂

budget for this region. For this simulation, both biological heterogeneity and meteorological factors had very significant impacts on the regional-scale patterns of CO₂ concentration.

[38] Gerbig *et al.* [2003] investigated representativeness error for a series of airborne measurements in August 2000, and found a relatively smooth increase in spatial variance that reached about 3 ppm at scales of 500 km. We find

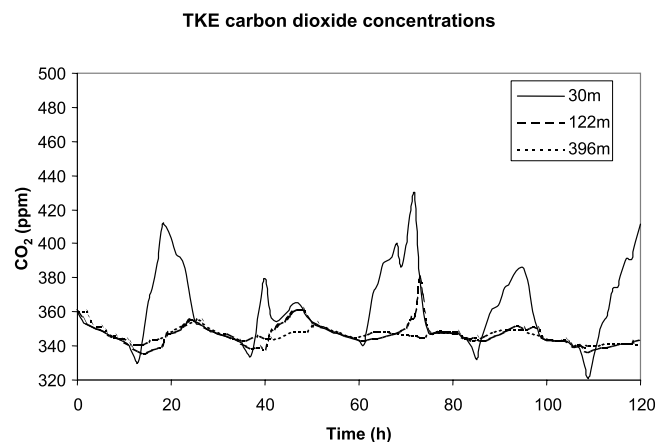


Figure 16. CO₂ concentrations at three levels using the turbulent kinetic energy subgrid-scale schemes.

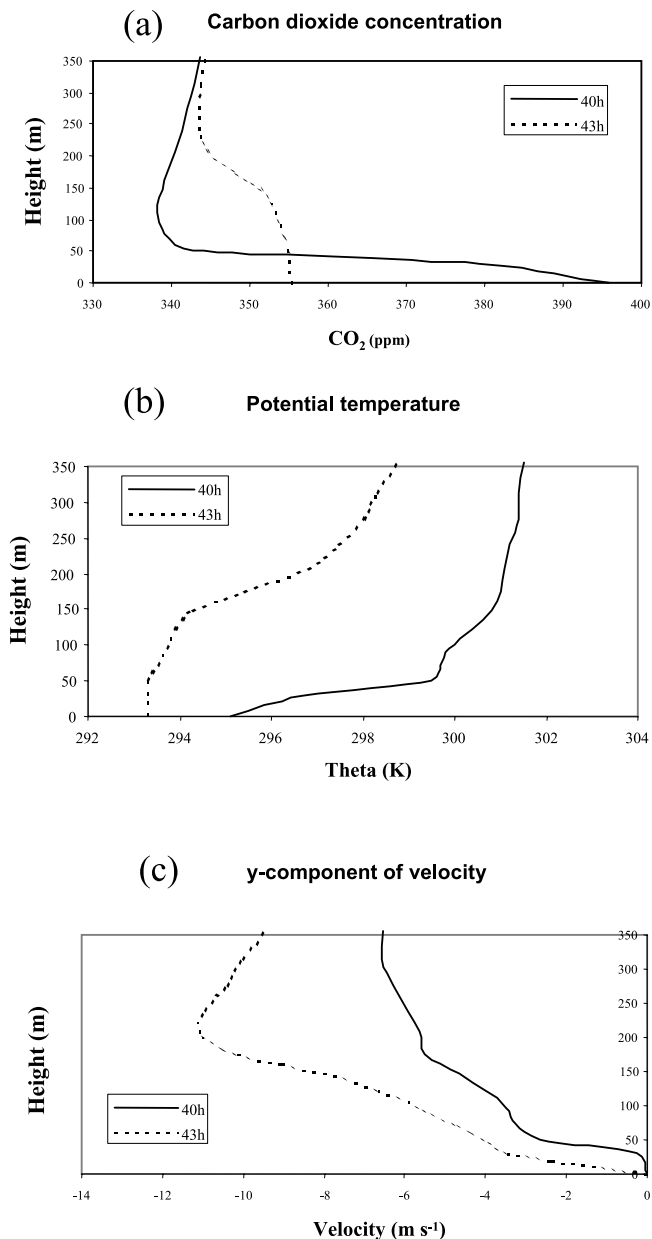


Figure 17. Vertical profiles of (a) CO₂, (b) potential temperature, and (c) y component of velocity at 40 h and 43 h.

substantially larger variations at both smaller and larger scales, related to the presence of cold lake surfaces, topography, and regional circulations. Such variations will certainly pose a challenge for inversions of continuous tower or periodic aircraft data.

[39] The simulations with cloud microphysics activated produced early morning fog on two of the days, which was not observed, and which was caused by the excessive nighttime cooling. The model was successful in producing shallow cumulus clouds, although they were not as frequent as they appeared to be from observations. The circulations associated with the clouds contributed to CO₂ variability. Boundary layer thermals typically produced CO₂ variations of 1–2 ppm, whereas when shallow cumulus clouds

occurred anomalies were usually larger (3–4 ppm), particularly in the cloudy air at the top of the boundary layer. Another way in which clouds can contribute to CO₂ variability is by shading the ground, which can effect the rate of photosynthesis. Shading reduces the direct radiation reaching the vegetation and may lead to a reduction in photosynthesis. In some circumstances cooler surface temperatures produced by shading may provide relief to stressed vegetation. For the small and scattered transient clouds simulated in this study these did not appear to be very significant effects. However for more abundant small clouds or large longer-lived clouds these effects could be considerable. An interesting study by *Freedman et al.* [2001] has shown that photosynthesis can be stimulated in forest canopies by the presence of boundary layer cumulus clouds leading to enhanced carbon uptake. They conclude that boundary layer cumulus can provide an additional source of diffuse radiation that penetrates deeper into the forest canopy. An important aspect of future modeling efforts which examine the influence of clouds, would be to implement a radiation scheme that is able to realistically model the scattering properties of air and clouds.

[40] This study also investigated the sensitivity to the subgrid-scale turbulence model employed. The two TKE options available in RAMS are more sophisticated subgrid-scale parameterizations than the deformation scheme. However, they are applicable to different scales and neither of them were designed to be used for scales of approximately 500 m to 5 km. It was found that the best combination was to use the Mellor-Yamada scheme on grids 1–3 and the Deardorff scheme on grid 4. Increased vertical mixing occurred in grid 4 with the Deardorff scheme employed compared to the deformation scheme, which gave better agreement with the observed vertical structure of CO₂ concentrations. However, the fields did not look as smooth, and when the cloud microphysics option was activated this scheme demonstrated considerable numerical noise within cloudy regions.

[41] This study demonstrates the feasibility of using multiple nested grid coupled biosphere-atmospheric models to interpret CO₂ variability at observation sites. Model output may be useful for determining the flux footprint of the WLEF-TV tower, for spatial scaling of CO₂ flux observations, and for evaluating regional-scale simulations. Future, longer duration regional-scale simulations will need to employ convective parameterizations that include vertical CO₂ transports and realistically incorporate cloud and radiation interactions. Cloud resolving simulations such as used in this study could aid in the development of these schemes. It is possible that as well as using regional models for CO₂ transport in future regional-scale inversion studies, that additional model fields such as surface CO₂ flux, could be used to provide further constraints to improve the accuracy of CO₂ source and sink predictions.

[42] **Acknowledgments.** Discussions with Robert Walko, Glen Liston, Neil Suits, and Roger Pielke Sr. are appreciated. Thanks to John Kleist for providing computational assistance and Connie Uliasz for helping prepare this manuscript. This research was funded in part by the South-Central Regional Center (SCRC) of the National Institute for Global Environmental Change (NIGEC) through the U.S. Department of Energy (cooperative agreement TUL-106-00/01 Mod 1. Support was also provided by NSF contract DEB-9977066 and Harvard subcontract under the project entitled CO₂ Budget and Rectification Airborne Study- North America. The

carbon dioxide mixing ratio measurements, and site infrastructure and maintenance at WLEF were supported by the Atmospheric Chemistry Project of the Climate and Global Change Program of the National Oceanic and Atmospheric Administration. Observations of NEE at WLEF were funded in part by the National Institute for Global Environmental Change through the U.S. Department of Energy through a grant to the University of Colorado. Any opinions, findings and conclusions or recommendations expressed herein are those of the authors and do not necessarily reflect the view of the DOE.

References

- Baker, I. T., A. S. Denning, N. Hanan, L. Prihodko, P.-L. Vidale, K. Davis, and P. Bakwin (2003), Simulated and observed fluxes of sensible and latent heat and CO₂ at the WLEF-TV Tower using SiB2.5, *Global Change Biol.*, *9*, 1262–1278.
- Bakwin, P. S., P. P. Tans, D. F. Hurst, and C. Zhao (1998), Measurements of carbon dioxide on very tall towers: Results of the NOAA/CMDL program, *Tellus, Ser. B*, *50*, 401–415.
- Berger, B. W., K. J. Davis, P. S. Bakwin, C. Yi, and C. Zhao (2001), Long-term carbon dioxide fluxes from a very tall tower in a northern forest: Flux measurement methodology, *J. Oceanic Atmos. Technol.*, *18*, 529–542.
- Bonan, G. B. (1996), A land surface model (LSM version 1.0) for ecological, hydrological, and atmospheric studies: Technical description and user's guide, *NCAR Tech. Note NCAR/TN-417+STR*, Natl. Cent. for Atmos. Res., Boulder, Colo.
- Clapp, R. B., and G. M. Hornberger (1978), Empirical equations for some soil hydraulic properties, *Water Resour. Res.*, *14*, 601–604.
- Clark, T. L. (1977), A small-scale dynamic model using a terrain-following coordinate transformation, *J. Comput. Phys.*, *24*, 186–215.
- Clark, T. L., and R. D. Farley (1984), Severe downslope windstorm calculations in two and three spatial dimensions using anelastic interactive grid nesting: A possible mechanism for gustiness, *J. Atmos. Sci.*, *41*, 329–350.
- Costigan, K. R. (1992), Large eddy simulations of the atmospheric boundary layer east of the Colorado Rockies, Ph.D. thesis, Colo. State Univ., Fort Collins.
- Cotton, W. R., et al. (2003), RAMS 2001: Current status and future directions, *Meteorol. Atmos. Phys.*, *82*, 5–29.
- Davies, H. C. (1983), Limitations of some common lateral boundary schemes used in regional NWP models, *Mon. Weather Rev.*, *111*, 1002–1012.
- Davis, K. J., P. S. Bakwin, C. Yi, B. W. Berger, C. Zhao, R. M. Teclaw, and J. G. Isebrands (2003), The annual cycles of CO₂ and H₂O exchange over a northern mixed forest as observed from a very tall tower, *Global Change Biol.*, *9*, 1278–1293.
- Deardorff, J. W. (1980), Stratocumulus-capped mixed layers derived from a three-dimensional model, *Boundary Layer Meteorol.*, *18*, 495–527.
- Denning, A. S., G. J. Collatz, and C. Zhang (1996), Simulations of terrestrial carbon metabolism and atmospheric CO₂ in a general circulation model. Part 1: Surface carbon fluxes, *Tellus, Ser. B*, *48*, 521–542.
- Denning, A. S., M. Nicholls, L. Prihodko, I. Baker, P.-L. Vidale, K. Davis, and P. Bakwin (2003), Simulated and observed variations in atmospheric CO₂ over a Wisconsin forest, *Global Change Biol.*, *9*, 1241–1250.
- Engelen, R. J., A. S. Denning, and K. R. Gurney (2002), On error estimation in atmospheric CO₂ inversions, *J. Geophys. Res.*, *107*(D22), 4635, doi:10.1029/2002JD002195.
- Freedman, J. M., D. R. Fitzjarrald, K. E. Moore, and R. K. Sakai (2001), Boundary layer clouds and vegetation-atmosphere feedbacks, *J. Clim.*, *14*, 180–197.
- Gal-Chen, T., and R. C. J. Somerville (1975), Numerical solution of the Navier-Stokes equations with topography, *J. Comput. Phys.*, *17*, 276–310.
- Gerbig, C., J. C. Lin, S. C. Wofsy, B. C. Daube, A. E. Andrews, B. B. Stephens, P. S. Bakwin, and C. A. Grainger (2003), Toward constraining regional-scale fluxes of CO₂ with atmospheric observations over a continent: 1. Observed spatial variability from airborne platforms, *J. Geophys. Res.*, *108*(D24), 4756, doi:10.1029/2002JD003018.
- Gurney, K. R., et al. (2003), TransCom3 CO₂ inversion intercomparison: 1. Annual mean control results and sensitivity to transport and prior flux information, *Tellus, Ser. B*, *55*, 555–579.
- Hansen, M. C., R. S. DeFries, J. R. G. Townshend, and R. Sohlberg (2000), Global land cover classification at 1 km spatial resolution using a classification tree approach, *Int. J. Remote Sens.*, *21*(6), 1331–1364.
- Hill, G. E. (1974), Factors controlling the size and spacing of cumulus clouds as revealed by numerical experiments, *J. Atmos. Sci.*, *31*, 646–673.
- Hollinger, D. Y., F. M. Kelliher, J. N. Byers, J. E. Hunt, T. M. McSeveny, and P. L. Weir (1994), Carbon dioxide exchange between an undisturbed old-growth temperate forest and the atmosphere, *Ecology*, *75*, 134–150.
- Intergovernmental Panel on Climate Change (2001), *Climate Change 2001: The Scientific Basis. Contribution of Working Group I to the Third Assessment Report of the Intergovernmental Panel on Climate Change*, edited by J. T. Houghton et al., 944 pp., Cambridge Univ. Press, New York.
- Jarvis, P. G., J. M. Massheder, S. E. Hale, J. B. Moncrieff, M. Rayment, and S. L. Scott (1997), Seasonal variations of carbon dioxide, water vapor, and energy exchanges of a boreal spruce forest, *J. Geophys. Res.*, *102*, 28,953–28,966.
- Klemp, J. B., and R. B. Wilhelmson (1978), The simulation of three-dimensional convective storm dynamics, *J. Atmos. Sci.*, *35*, 1070–1086.
- Lavigne, M. B., et al. (1997), Comparing nocturnal eddy covariance measurements to estimates of ecosystem respiration made by scaling chamber measurements at six coniferous boreal sites, *J. Geophys. Res.*, *102*, 28,799–28,985.
- Lee, X. (1998), On micrometeorological observations of surface-air exchange over tall vegetation, *Agric. For. Meteorol.*, *91*, 39–49.
- Lilly, D. K. (1962), On the numerical simulation of buoyant convection, *Tellus*, *14*, 148–172.
- Los, S. O., et al. (2000), A global 9-yr biophysical land surface dataset from NOAA AVHRR data, *J. Hydrometeorol.*, *1*(2), 183–199.
- Mellor, G. L., and T. Yamada (1982), Development of a turbulence closure model for geophysical fluid problems, *Rev. Geophys.*, *20*, 851–875.
- Nicholls, M. E., R. A. Pielke, J. L. Eastman, C. A. Finley, W. A. Lyons, C. J. Treback, R. L. Walko, and W. R. Cotton (1995), Applications of the RAMS numerical model to dispersion over urban areas, in *Wind Climate in Cities*, edited by J. E. Cermak et al., pp. 703–732, Kluwer Acad., Norwell, Mass.
- Pielke, R. A., et al. (1992), A comprehensive meteorological modeling system RAMS, *Meteorol. Atmos. Phys.*, *49*, 69–91.
- Sellers, P. J., Y. Mintz, Y. C. Sud, and A. Dalcher (1986), A simple biosphere model (SiB) for use within general circulation models, *J. Atmos. Sci.*, *43*, 505–531.
- Sellers, P. J., D. A. Randall, G. J. Collatz, J. Berry, C. Field, D. A. Dazlich, C. Zhang, and L. Bounoua (1996a), A revised land-surface parameterization (SiB2) for atmospheric GCMs. Part 1: Model formulation, *J. Clim.*, *9*, 676–705.
- Sellers, P. J., S. O. Los, C. J. Tucker, C. O. Justice, D. A. Dazlich, G. J. Collatz, and D. A. Randall (1996b), A revised land-surface parameterization (SiB2) for atmospheric GCMs. Part 2: The generation of global fields of terrestrial biophysical parameters from satellite data, *J. Clim.*, *9*, 706–737.
- Smagorinsky, J. S. (1963), General circulation experiments with the primitive equations. 1: The basic experiment, *Mon. Weather Rev.*, *91*, 99–164.
- Soil Survey Staff (1994), State Soil Geographic Database (STATSGO), Nat. Resour. Conserv. Serv., U.S. Dep. of Agric., Fort Worth, Tex.
- Sun, J., R. Desjardins, L. Mahrt, and I. MacPherson (1998), Transport of carbon dioxide, water vapor, and ozone by turbulence and local circulations, *J. Geophys. Res.*, *103*, 25,873–25,885.
- Tans, P. P., I. Y. Fung, and T. Takahashi (1990), Observational constraints on the global atmospheric CO₂ budget, *Science*, *247*, 1431–1438.
- Teillet, P. M., N. El Saleous, M. C. Hansen, J. C. Eidsensink, C. O. Justice, and J. R. G. Townshend (2000), An evaluation of the global 1-Km AVHRR land dataset, *Int. J. Remote Sens.*, *21*(10), 1987–2021.
- Wofsy, S. C., and R. C. Harriss (2002), The North American Carbon Program (NACP), report, U.S. Global Change Res. Program, Washington, D. C. (Available at <http://www.carboncyclescience.gov/nacp.pdf>)

I. Baker, A. S. Denning, M. E. Nicholls, and L. Prihodko, Department of Atmospheric Science, Colorado State University, Fort Collins, CO 80523-1371, USA. (nicholls@atmos.colostate.edu)

P. Bakwin, Climate Monitoring and Diagnostics Laboratory, NOAA, Boulder, CO 80305, USA.

K. Davis, Department of Meteorology, Pennsylvania State University, University Park, PA 16802-5013, USA.

P.-L. Vidale, Institute for Atmospheric and Climate Science, ETH Zurich, CH-8092 Zurich, Switzerland.